
Generalizable Human Gaussians from Single-View Image

Jinnan Chen¹ Chen Li¹ Jianfeng Zhang² Hanlin Chen¹ Buzhen Huang¹ Gim Hee Lee¹

¹ School of Computing, National University of Singapore

² Bytedance

<https://github.com/jinnan-chen/HGM>

Abstract

In this work, we tackle the task of learning generalizable 3D human Gaussians from a single image. The main challenge for this task is to recover detailed geometry and appearance, especially for the unobserved regions. To this end, we propose single-view generalizable Human Gaussian model (HGM), a diffusion-guided framework for 3D human modeling from a single image. We design a diffusion-based coarse-to-fine pipeline, where the diffusion model is adapted to refine novel-view images rendered from a coarse human Gaussian model. The refined images are then used together with the input image to learn a refined human Gaussian model. Although effective in hallucinating the unobserved views, the approach may generate unrealistic human pose and shapes due to the lack of supervision. We circumvent this problem by further encoding the geometric priors from SMPL model. Specifically, we propagate geometric features from SMPL volume to the predicted Gaussians via sparse convolution and attention mechanism. We validate our approach on publicly available datasets and demonstrate that it significantly surpasses state-of-the-art methods in terms of PSNR and SSIM. Additionally, our method exhibits strong generalization for in-the-wild images.

1 Introduction

Automatic 3D human reconstruction from single image is crucial in augmented and virtual reality (AR/VR), game industry, filmmaking, *etc.* Previous works either rely on strong 3D supervision such as groundtruth signed distance value [23, 24, 39, 30, 29, 40, 9], or extra input [30, 29, 40, 9] such as normal and depth. However, most of them focus on surface geometry rather than novel view synthesis quality. With the development of neural radiance fields [20], novel view rendering quality has been greatly improved with multi-view posed images. SHERF [11] is proposed to predict human radiance fields from a single image. However, the back and side views are always blurry and lack details without additional prior. Furthermore, it needs large amounts of query points sampled for volume rendering, which hinders practical real-time application in the industries. 3D contents generation has been significantly boosted with the help of pre-trained diffusion models. Some methods optimize underlying geometry from scratch by introducing score distillation sampling during the optimization. Although effective, these methods still suffer from long time optimization and over-saturation problems. Recent 3D Gaussians generation methods [27, 35] combine multi-view diffusion models [18, 28, 25, 3, 33] with generalizable multi-view Gaussians prediction models to generate 3D Gaussians with high quality and efficiency. We aim to extend this on human reconstruction. However, directly employ such methods to human images with complex texture and poses may give unsatisfying results due to: 1) Original input image are down-sampled and then regenerated with multi-view diffusion models, leading to severe quality degradation of the front view image. 2) Inconsistency between training and inference. Specifically, the input multi-view images are ground-truth images with accurate camera poses and multi-view consistency during training. On the

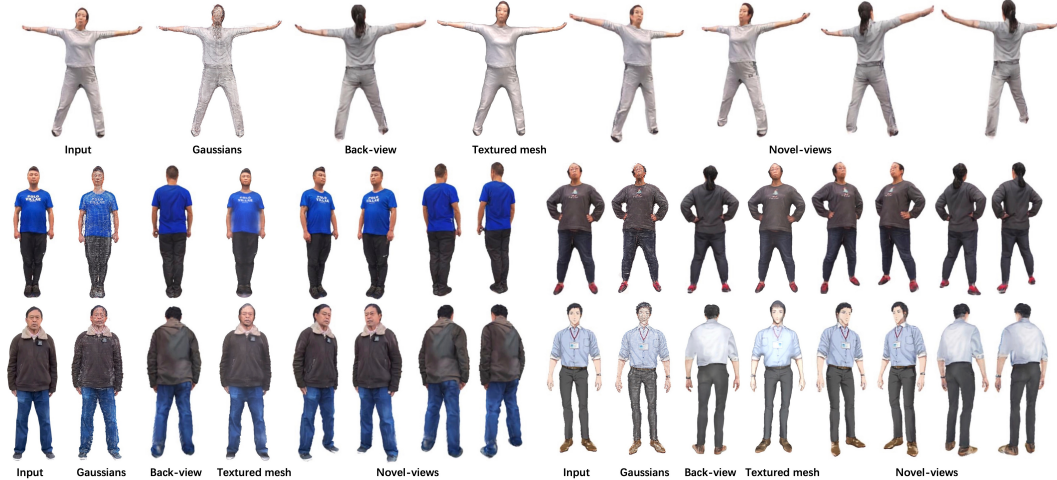


Figure 1: Our reconstructed Gaussians, refined back-view, extracted textured mesh and novel view synthesis from single view images, including in the wild images and OOD images in the last row.

other hand, the generated multi-view images from image can be inconsistent and the camera poses can deviate from the training settings during inference. To address the above-mentioned problems, we introduce a novel Human Gaussians Model (HGM) with Gaussians splatting, which support fast and high quality rendering from single view input in 180 FPS, and generalize well to in-the-wild cartoon images as shown in Fig 1. We do not use multi-view diffusions on the consideration of the inconsistency problem.

Instead, we propose a diffusion based coarse-to-fine framework, where the diffusion model is adapted to refine back-view images rendered from a coarse human Gaussian model. We inject human prior to the Gaussian prediction process for generalization ability in terms of different poses. Specifically, our model consists of two branches: 1) The first branch is a UNet to directly predict the Gaussians from the input image, as inspired by image splatter [26]. 2) The second branch predicts Gaussians based on the predicted/fitted SMPL vertices with projected image features due to the depth ambiguity and complexity of the human pose. Although the SMPL predicted Gaussians are enhanced with human pose and shape prior, the generated Gaussians are still blurry when trained with limited data. To distill the human prior from the SMPL predicted Gaussians and to overcome the difficulty to register two branches of Gaussians, we do a soft combination of the two Gaussians by diffusing the SMPL Gaussians features to the bounding box and resample the diffused SMPL volume feature with the mean of the UNet predicted Gaussians. As a result, the SMPL predicted Gaussians correct the wrong depth and pose of the UNet predicted Gaussians without losing its high-frequency details. Subsequently, we combine the feature from two branches and input them into a transformer to predict the final Gaussians. Given the loss of details of the back-view by directly predicting the Gaussians from a single view, we further apply pre-trained diffusion models to refine the back view. We then input the original front view and refined back view images to our two-view model with additional cross-view self-attentions to get the final output. Meshes can be extracted from densely rendered depth map with Gaussians renderer and TSDF fusion. Our model can be trained with only posed multi-view images without any 3D supervision and generalize well to in the wild images, even for human images in different domains such as cartoon characters.

In summary, our contributions are:

- To the best of our knowledge, we are first to propose a generalizable feed-forward human Gaussian reconstruction framework from single image.
- We design a method to inject human prior into a generalizable Gaussian model to better infer human geometry and texture while keeping multi-view consistency and high fidelity.
- We conduct extensive experiments to demonstrate the effectiveness of our method in both novel view synthesis and 3D reconstruction.

2 Related works

Single-view Human Reconstruction. PIFu [23], PIFuHD [24], PaMIR [42], and GTA [39] are capable of inferring full textures from a single image. Techniques such as PHORHUM [2] and S3F [6] go further by separating albedo and global illumination. However, these methods lack information from other views or prior knowledge, such as diffusion models, often resulting in unsatisfactory textures. TeCH [14] utilizes diffusion-based models for visualizing unseen areas, producing realistic results. However, it requires time-intensive per-subject optimization and depends on accurate SMPL-X. The emergence of Neural Radiance Fields (NeRF) has led to methods [11, 13, 7, 17] using videos or multi-view images to optimize NeRF for human form capture. Recent advancements like SHERF [11] and ELICIT [13] aim to generate human NeRFs from single images. While NeRF-based approaches are effective in creating high-quality images from various perspectives, they often struggle with detailed 3D mesh generation from single images and require extensive optimization time. More recently, SiTH [9] proposes to combine a back-view hallucination model with an SDF-based mesh reconstruction model. Similarly, SiFU [40] employs a text-to-image diffusion-based prior to generate realistic and consistent textures for invisible views. However, these methods require 3D annotations such as the SDF of the meshes and texture maps as strong supervision, which are not always available. Compared to these methods, our approach can be trained solely on multi-view images and achieves better performance and generalize well to in-the-wild images.

Human Gaussians. 3D Gaussians [15] and differentiable splatting [26] have gained broad popularity due to their efficiency in reconstructing high-fidelity 3D scenes from posed images using only a moderate number of 3D Gaussians. This representation has been quickly adopted for various applications, including image or text-conditioned 3D generation and avatar reconstruction. Among these methods, GauHuman and HUGS [12, 16] are first to propose optimizing human Gaussians from monocular human videos. However, they are not applicable to single static human images. GPS-Gaussian[41] propose a generalizable multi-view human Gaussian model with high quality rendering, however, it need dense views 16 or 8, which can not be directly applied to single view human images. In contrast, our human model is able to generate Gaussians from single view images with strong generalization.

Generalizable Gaussians with Multi-view Diffusion. The Large Reconstruction Model (LRM) [10] scales up both the model and the dataset to predict a neural radiance field (NeRF) from single-view images. Although LRM is primarily a reconstruction model, it can be combined with Diffusion Models (DMs) to achieve text-to-3D and image-to-3D generation as demonstrated by extensions such as Zero123[18], Image Dream[28] Instant3D [3] and DMV3D [33]. Our method also builds on a strong reconstruction model and uses pretrained 2D DMs to provide input images missing information in a feed-forward manner. Some concurrent works, such as LGM [27], AGG [31], and Splat Image [26], also utilize 3D Gaussians in a feed-forward model. LGM [27] combines novel view generation diffusion models with generalizable Gaussians in a feed-forward manner, while GRM [35] replaces the U-Net architecture with a pure-transformer one and scales up to large resolution. However, these methods face two main challenges when using pre-trained diffusion models. Firstly, the generated input view image becomes blurry compared to the original input, which affects the subsequent generalizable Gaussian model. Secondly, diffusion models can introduce multi-view inconsistency, especially for human images with different poses, making direct adaptation unfeasible. We solve these problems by only using DMs as the refine tools without damage the input image quality or introducing multi-view inconsistency. We adopt highly efficient 3D Gaussians[15] for representing and rendering. This design alleviates the computation and memory bottleneck posed by NeRF and volumetric rendering, enabling us to generate high-quality 3D avatars within seconds.

3 Our Method

3.1 Preliminaries

3D Gaussian Splatting (3DGS). Introduced by [15], 3D Gaussian splatting represents 3D assets or scenes using a collection of 3D Gaussians. Each Gaussian is characterized by its center $x \in \mathbb{R}^3$, scaling factor $s \in \mathbb{R}^3$, rotation $r \in \mathbb{R}^3$, opacity $\alpha \in \mathbb{R}$, and color feature $c \in \mathbb{R}^c$. View-dependent effects can be modeled with spherical harmonics. A 3D scene can thus be represented explicitly by a set of Gaussians $G = \{G_i\}$, where $G_i = \{x_i, s_i, r_i, \alpha_i, c_i\}$ represents the attributes for the i -th

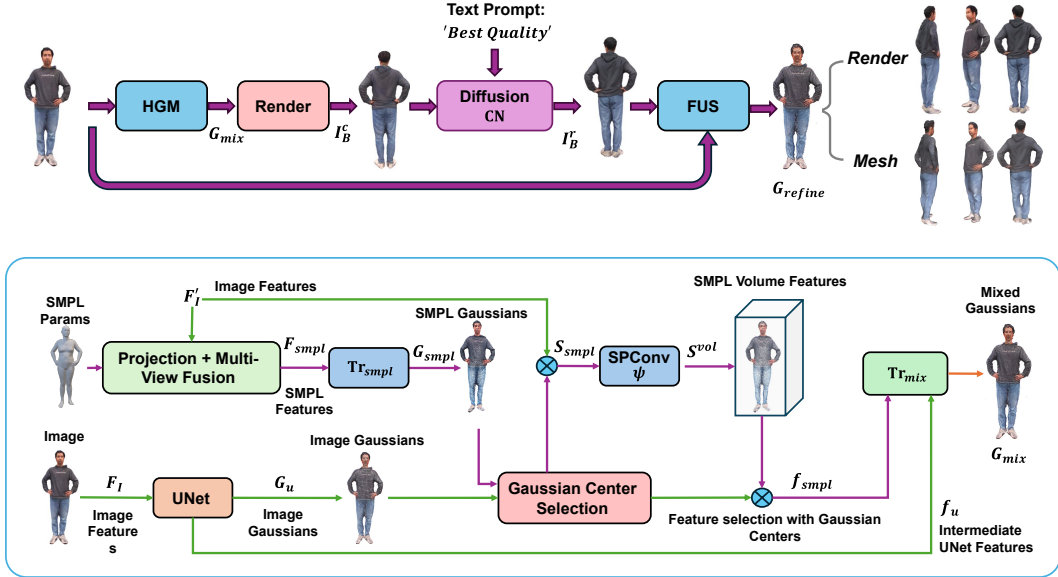


Figure 2: Our framework and HGM model. (Top) Our framework consists of three steps: 1) Coarse Gaussians prediction with human prior by HGM. 2) Back view refinement with diffusion models. 3) Two view reconstruction to get the refined G_{refine} . (Bottom) Our HGM model consists of two branches of Gaussians prediction by UNet and Tr_{smpl} . Features f_{smpl} and f_u sampled by the Gaussian centers from the SMPL G_{smpl} and image G_u branches are then fused to get the final output.

Gaussian. Compared with NeRF [20], 3DGS performs fast rendering by first projecting Gaussians onto the image plane as 2D Gaussians and performing alpha-blending for each pixel in a front-to-back depth order. Building on this, Image Splatter [26] proposes predicting Gaussians from a single image through image-to-image translation. Specifically, each pixel is converted to a Gaussian with corresponding attributes, supervised by multi-view images. The Gaussians center are represented by unprojected pixels with predicted depth. Our model builds on this representation by directly predicting XYZ coordinates from the image instead of depth.

3.2 Overview

Fig. 2 shows an overview of our framework. Given single input human image I , our aim is to predict the corresponding human Gaussians G , which can be further rendered for novel view synthesis and mesh extraction. As shown in the upper part of Fig. 2, our proposed method consists of three parts: 1) **Coarse Gaussians prediction with human prior by HGM** (cf. Sec. 3.3). We utilize human shape and pose prior from SMPL as guidance to provide additional feature for the coarse Gaussian prediction. 2) **Back-view refinement with diffusion models** (cf. Sec. 3.4). Gaussians predicted by the front-view are always blurry and lack details, we add this part to enrich the back-view details. 3) **Two-view reconstruction** (cf. Sec. 3.5). We put the images from both views our fusion reconstruction module (a slight modification of HGM with cross-attention) to get the final refined Gaussians.

3.3 Coarse Gaussians Prediction with Human Prior by HGM

The lower part of Fig. 2 shows our proposed Human Gaussian Model (HGM). The direct prediction of Gaussians from image pixels with UNet [26, 27] lacks human shape and pose prior, thus leading to unsatisfactory results. We therefore introduce a second branch that utilizes SMPL to enforce human shape and pose prior into the Gaussian predictions. Specifically, for UNet branch, the collection of the RGB value and ray embedding for each pixel are concatenated into a 9-channel feature map as the input $F_I = \{c_i, o_i \times d_i, d_i \mid i = 1, 2, \dots, N\}$. Our HGM model predicts Gaussians from the UNet as:

$$G_u = \text{UNet}(F_I), \quad (1)$$



Figure 3: Our back-view refinement results.

For SMPL branch, we first densify the SMPL vertices by adding the mean of each edge and the center of each face in the SMPL mesh to get a dense feature volume. We then extract images features F'_I with another shallow UNet for G_{smpl} prediction. We project F'_I from K input views to each vertices as F_q^k , where $q = 1, 2, \dots, N_{smpl}, k = 1, \dots, K$. $K = 1$ for coarse gaussian prediction and $K = 2$ for two-view reconstruction. To merge features from different views, we follow [5] to use a view-attention block to aggregate them: $F_{smpl} = \{F_q \mid q = 1, 2, \dots, N_{smpl}\}$, where $F_q = \text{Att}(F_q^1, F_q^2, \dots, F_q^K)$. The merged features are subsequently used to predict the coordinates residuals for the densified SMPL vertices and other Gaussian features with:

$$G_{smpl} = \text{Tr}_{smpl}(F_{smpl}), \quad (2)$$

where $G_{smpl}^i = \{\Delta x_i, s_i, r_i, \alpha_i, c_i\}$. G_{smpl} ensures the coverage of finer details such as clothes and hair in the reconstruction. We observed that while G_u provides better texture details, it lacks the human shape and pose priors that G_{smpl} can offer. To address this issue, we apply the SparseConvNet [8] (SPConv Ψ) to propagate SMPL features to the whole bounding box, and we denote this feature as the SMPL volume feature: $S^{vol} = \Psi(S_{smpl})$, where S_{smpl} are features sampled by the center C_{smpl} of G_{smpl} . Note that S_{smpl} and F_{smpl} are sampled from F'_I . The volume feature reconstructed from the SMPL vertex feature provides geometric cues of the target human body. The centers of the Gaussians from G_u are then used to sample the propagated SMPL volume features, denoted as $f_{smpl} = S^{vol}(C_u)$, where C_u are the centers of G_u . The sampled SMPL features are then concatenated with the intermediate features from the UNet f_u for each Gaussian. This concatenated feature is fed into another transformer Tr_{mix} to obtain the mixed Gaussians:

$$G_{mix} = \text{Tr}_{mix}([f_u, f_{smpl}]). \quad (3)$$

Both Tr_{smpl} and Tr_{mix} contain multiple self-attention blocks among the Gaussians to ensure that each Gaussian is aware of the other.

3.4 Back-view Refinement

Back-view hallucination poses a significant challenge in single-view human reconstruction. As shown in Fig. 3, directly using diffusion models to generate a back-view image can result in incorrect perspective projection with the front-view image [9]. The reason is that their diffusion is conditioned on the back-view mask, and thus can only be applied for orthogonal projection when directly flipped with the front-view image. However, the back-view mask is not available during our inference stage since our prediction is based on perspective projection. To address this issue, we adopt a generate-then-refine strategy that leverages both front and back views, and the diffusion prior to produce a perspective-fitted and realistic back-view image that is suitable for the subsequent two-view fusion stage. Specifically, we use the ControlNet [37] tile model, which enhances realistic details based on our coarse results instead of merely performing super-resolution. Specifically,

$$I_B^r = \text{CN}(y, I_B^c), \quad (4)$$

where y is the prompt set as ‘Best quality’, I_B^c and I_B^r are back-view image before and after refinement, the controlnet condition and input image are the same coarse back-view image, the sampling strength as 0.5 and sampling steps as 30. The sampling process takes around 4 seconds. In

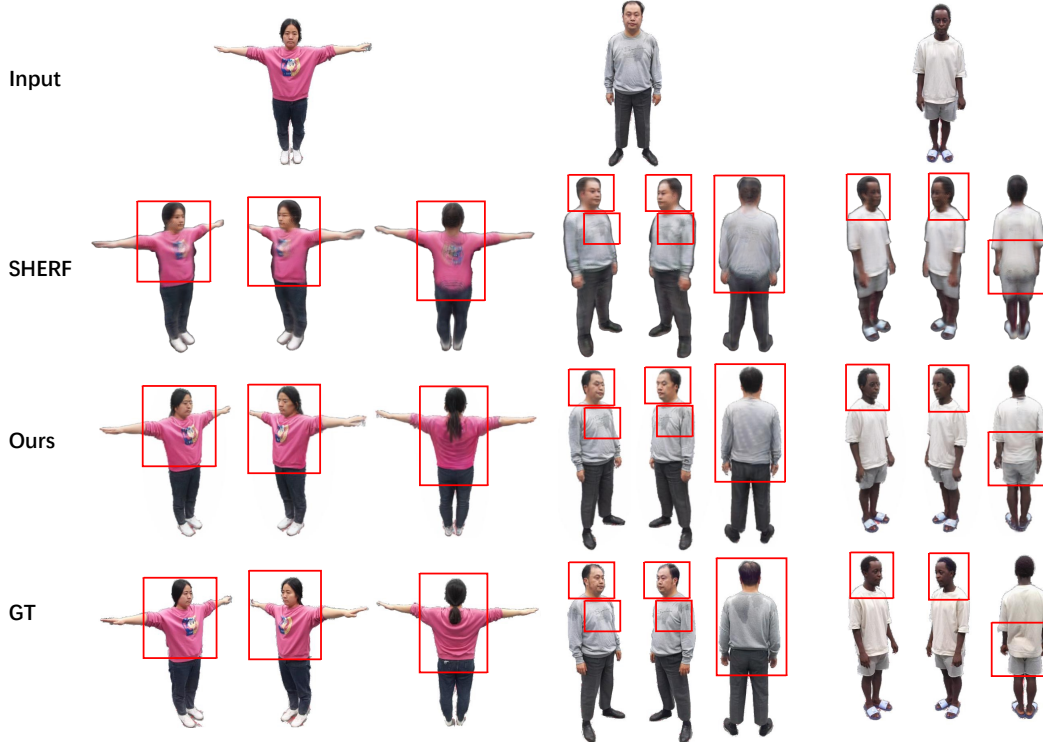


Figure 4: Novel view synthesis comparison with SHERF on HuMMan dataset. The details are highlighted in the red boxes.

Fig. 3, we showcase our generated and refined back-view results, comparing them with the back-view hallucination diffusion network in SiTH [40]. Our results maintain high resolution and generate details such as the hair for the first woman and the wrinkles in the clothes, whereas SiTH [40] produces less detailed results that are not perspective-fitted to the input image.

3.5 Two-view Reconstruction

We combine the refined perspective-fitted back-view image I_B^r with the front-view image I and input them into the fusion reconstruction model to get:

$$G_{refine} = \text{FUS}(I, I_B^r). \quad (5)$$

Specifically, our fusion model retains the design of the coarse Gaussians prediction HGM model, but modifies the original single-view Gaussian self-attention to cross-view attention. The cross-attention allows the Gaussians predicted from both views to be aware of each other. Additionally for the SMPL branch, we get the projected features from both views and perform a view attention to learn to select features from the correct view.

3.6 Losses and Implementation

Our complete objective function includes the L2 color loss, \mathcal{L}_{rgb} , the VGG-based LPIPS perceptual loss, \mathcal{L}_{lpiPs} [38], and the L2 background mask loss with ground truth masks, \mathcal{L}_{bg} . Each of these losses has corresponding weights that are treated as hyperparameters:

$$\mathcal{L} = \lambda_{rgb}\mathcal{L}_{rgb} + \lambda_{lpiPs}\mathcal{L}_{lpiPs} + \lambda_{bg}\mathcal{L}_{bg}, \quad (6)$$

where $\lambda_{rgb} = \lambda_{lpiPs} = \lambda_{bg} = 1.0$. We separately train UNet and Tr_{smpl} , and jointly train with Tr_{mix} on 4 NVIDIA RTX A6000 with batch size of 4 for 20 hours. Our input image size is 512×512 , and the number of Gaussians for each view is 256×256 , totaling 65,536 Gaussians per view. For UNet, we use [27] pre-trained model as initialization. For SMPL estimation, we use SMPLER[32]. Network structures are in the supplementary materials.

4 Experiments

We conduct experiments on the publicly available 3D human datasets THuman2.0 [36] and HuMMan [4]. Our method is compared with state-of-the-art (SOTA) methods in both novel view synthesis and 3D mesh reconstruction.

Table 1: Novel view synthesis comparison with SOTA HumanNeRF methods on HuMMan.

Method	PSNR \uparrow	SSIM \uparrow	LPIPS \downarrow
NHP [17]	18.99	0.84	0.18
MPS-NeRF [7]	17.44	0.82	0.19
SHERF [11]	20.83	0.89	0.12
Ours	23.86	0.95	0.062

4.1 Novel View Synthesis

For novel view synthesis, we compare our method with state-of-the-art HumanNeRF methods: SHERF [11], MPS-NeRF [7], and NHP [17] on the HuMMan dataset [4]. Additionally, we compare our method with mesh reconstruction methods PIFu [23], S3F [6], HumanSGD [1], and SiTH [9], as well as diffusion-guided reconstruction methods Magic123 [21] and TEXture [22] on the THuman2.0 dataset. We follow SHERF [11] and SIFU [40] to evaluate our method on HuMMan dataset and THuman2.0 dataset.

Table 2: Rendering speed comparison with NHP, MPS-NeRF, SHERF. ‘‘FPS’’ represents inference frames per second, the higher the better.

Method	NHP [17]	MPS-NeRF [7]	SHERF [11]	Ours
FPS	0.15	0.60	1.33	382

As shown in Table 1, our method significantly surpasses the state-of-the-art single-view HumanNeRF [11] by 14.5% in PSNR on the HuMMan dataset. We also present qualitative comparisons with the SOTA method SHERF and SIFU for both categories, respectively, in Fig. 4 and Fig. 5. While SHERF predicts blurry results and loses fidelity, our method preserves high-frequency details and generates realistic back-views such as wrinkles and hair that are well-fitted to the front views. This shows the effectiveness of our proposed framework in generating high quality unseen back-view while preserving the details of the front-view. SIFU predicts incorrect poses due to inaccurate SMPL estimation, and also loses texture details. In contrast, our method is more robust to SMPL estimation errors since we only use the SMPL-diffused feature volume to provide additional features implicitly. We also compare the rendering efficiency with NeRF-based methods in Table 2. Our method is around $300\times$ faster due to the Gaussians rendering. For cross-dataset evaluation, we train on THuman 2.0 and test on HuMMan dataset, and we include the rendered 360-degree video in the supplementary materials.

Table 3: Novel view synthesis comparison with SOTA mesh reconstruction methods on THuman2.0.

Method	PSNR \uparrow	SSIM \uparrow	LPIPS \downarrow
PIFu [23]	18.0934	0.9117	0.1372
Impersonator++[19]	16.4791	0.9012	0.1468
TEXture[22]	16.7869	0.8740	0.1435
Magic123[21]	14.5013	0.8768	0.1880
S3F [6]	14.1212	0.8840	0.1868
HumanSGD[1]	17.3651	0.8946	0.1300
SIFU[40]	22.1024	0.9236	0.0794
Ours w GT SMPL	23.7415	0.9560	0.0511
Ours w/o GT SMPL	22.5243	0.9356	0.0594

4.2 3D reconstruction

We also extract the 3D mesh by densely rendering the depth map with Gaussian render and using TSDFusion to extract the surface. We compare our results with SOTA human surface reconstruction



Figure 5: Novel view synthesis comparison with SiFU on THuman2.0 dataset. The details are highlighted in the red boxes.

Table 4: 3D reconstruction comparison with SOTA. Only our method trained *without* 3D supervision.

Method	Chamfer ↓	P2S ↓	Normal ↓
PiFu[23]	1.5991	1.4333	0.0843
PaMIR[42]	1.2152	1.0582	0.0730
ICON[30]	0.9491	0.9846	0.0621
ECON[29]	1.2585	1.4184	0.0612
D-IF[34]	1.1696	1.2900	0.0936
GTA[39]	0.7329	0.7297	0.0492
SiFU[40]	0.5961	0.6058	0.0407
Ours	0.8532	0.9323	0.0586

methods PiFu [23], Impersonator++ [19], ICON [30], ECON [29], D-IF [34], GTA [39], SiFU [40]. Following [40], we use Chamfer Distance (CD), Point-to-Surface Distance (P2S), and L2 normal map error as evaluation metrics. Note that our method do not use the 3D ground truth for supervision, but can also achieve satisfying results compared with all those fully supervised methods. We show the 3D reconstructed results with some in the wild images in Fig6, we can see our our model has strong generalization ability even though without post-optimization like [30, 29, 40].

Table 5: Ablation study for each component on THuman2.0 dataset .

Components	PSNR(↑)	SSIM(↑)	LPIPS(↓)
w/o SMPL guide	21.85	0.9303	0.619
w/o Two view refine	22.95	0.9322	0.656
w/o Diffusion	23.31	0.9352	0.639
Full model	23.74	0.9560	0.511



Figure 6: 3D reconstruction visualization for some in the wild images, the first row are input images, the second row are texture-less meshes and textured meshes

4.3 Ablation Studies

We conduct ablation studies to evaluate the effectiveness of our SMPL-guided Gaussian prediction model, coarse-to-fine refinement strategy, and diffusion model. As shown in Table 5, both PSNR and SSIM decrease when any component is removed. This shows the importance of SMPL guidance. The predicted Gaussians lack human shape and pose priors without SMPL guidance, resulting in unnatural shapes and poses. The visual comparisons of SMPL guidance are shown in the supplementary materials. The diffusion-based refinement is crucial for improving the quality of back-view images as shown in Fig. 3. Additionally, the Gaussians tend to concentrate more on the front view without the two-view refinement strategy, leading to poorer rendering of the back part. The best performance is achieved with all three components.

5 Conclusion

In this paper, we introduce a generalizable single-view human Gaussian reconstruction framework. By incorporating human priors and diffusion priors into the Gaussian prediction process, our method effectively handles invisible parts and varying poses. We validate the proposed method on several benchmarks and demonstrate that it achieves state-of-the-art performance in novel view synthesis and also show strong generalization ability for in the wild images.

Limitations Currently, our mesh extraction process is not end-to-end and the extracted meshes lacks surface regularization. As a result, the extracted meshes exhibit more noise compared to state-of-the-art single-view human mesh reconstruction methods [9, 40]. How to regularize Gaussians on the human surface is our future research.

Broader Impact This technology can revolutionize the creation of digital content in movies, video games, and virtual reality. It allows for the rapid and cost-effective generation of detailed 3D human models from a single image, enhancing the realism and diversity of virtual characters and scenes.

References

- [1] Badour AlBahar, Shunsuke Saito, Hung-Yu Tseng, Changil Kim, Johannes Kopf, and Jia-Bin Huang. Single-image 3d human digitization with shape-guided diffusion. In *SIGGRAPH Asia*, 2023.
- [2] Thiemo Alldieck, Mihai Zanfir, and Cristian Sminchisescu. Photorealistic monocular 3d reconstruction of humans wearing clothing. In *CVPR*, 2022.
- [3] Anonymous. Instant3d: Fast text-to-3d with sparse-view generation and large reconstruction model. *Under Review*, 2023.
- [4] Zhongang Cai, Daxuan Ren, Ailing Zeng, Zhengyu Lin, Tao Yu, Wenjia Wang, Xiangyu Fan, Yang Gao, Yifan Yu, Liang Pan, Fangzhou Hong, Mingyuan Zhang, Chen Change Loy, Lei Yang, and Ziwei Liu. HuMMan: Multi-modal 4d human dataset for versatile sensing and modeling. In *ECCV*, 2022.
- [5] Mingfei Chen, Jianfeng Zhang, Xiangyu Xu, Lijuan Liu, Yujun Cai, Jiashi Feng, and Shuicheng Yan. Geometry-guided progressive nerf for generalizable and efficient neural human rendering. In *ECCV*, 2022.
- [6] Enric Corona, Mihai Zanfir, Thiemo Alldieck, Eduard Gabriel Bazavan, Andrei Zanfir, and Cristian Sminchisescu. Structured 3d features for reconstructing relightable and animatable avatars. In *CVPR*, 2023.
- [7] Xiangjun Gao, Jiaolong Yang, Jongyoo Kim, Sida Peng, Zicheng Liu, and Xin Tong. Mps-nerf: Generalizable 3d human rendering from multiview images. In *PAMI*, 2022.
- [8] Benjamin Graham, Martin Engelcke, and Laurens van der Maaten. 3d semantic segmentation with submanifold sparse convolutional networks. In *CVPR*, 2018.
- [9] Hsuan-I Ho, Jie Song, and Otmar Hilliges. Sith: Single-view textured human reconstruction with image-conditioned diffusion. In *CVPR*, 2024.
- [10] Yicong Hong, Kai Zhang, Jiuxiang Gu, Sai Bi, Yang Zhou, Difan Liu, Feng Liu, Kalyan Sunkavalli, Trung Bui, and Hao Tan. Lrm: Large reconstruction model for single image to 3d, 2024.
- [11] Shoukang Hu, Fangzhou Hong, Liang Pan, Haiyi Mei, Lei Yang, and Ziwei Liu. Sherf: Generalizable human nerf from a single image. In *ICCV*, 2023.
- [12] Shoukang Hu and Ziwei Liu. Gauhuman: Articulated gaussian splatting from monocular human videos. In *CVPR*, 2024.
- [13] Yangyi Huang, Hongwei Yi, Weiyang Liu, Haofan Wang, Boxi Wu, Wenxiao Wang, Binbin Lin, Debing Zhang, and Deng Cai. One-shot implicit animatable avatars with model-based priors. In *ICCV*, 2023.
- [14] Yangyi Huang, Hongwei Yi, Yuliang Xiu, Tingting Liao, Jiaxiang Tang, Deng Cai, and Justus Thies. TeCH: Text-guided Reconstruction of Lifelike Clothed Humans. In *3DV*, 2024.
- [15] Bernhard Kerbl, Georgios Kopanas, Thomas Leimkühler, and George Drettakis. 3d gaussian splatting for real-time radiance field rendering. *ACM Transactions on Graphics*, 42(4), July 2023.
- [16] Muhammed Kocabas, Rick Chang, James Gabriel, Oncel Tuzel, and Anurag Ranjan. Hugs: Human gaussian splats, 2023.
- [17] Youngjoong Kwon, Dahun Kim, Duygu Ceylan, and Henry Fuchs. Neural human performer: Learning generalizable radiance fields for human performance rendering. *NIPS*, 2021.
- [18] Ruoshi Liu, Rundi Wu, Basile Van Hoorick, Pavel Tokmakov, Sergey Zakharov, and Carl Vondrick. Zero-1-to-3: Zero-shot one image to 3d object. In *ICCV*, 2023.
- [19] Wen Liu, Zhixin Piao, Min Jie, Wenhan Luo, Lin Ma, and Shenghua Gao. Liquid warping gan: A unified framework for human motion imitation, appearance transfer and novel view synthesis. In *ICCV*, 2019.
- [20] Ben Mildenhall, Pratul P. Srinivasan, Matthew Tancik, Jonathan T. Barron, Ravi Ramamoorthi, and Ren Ng. Nerf: Representing scenes as neural radiance fields for view synthesis. In *ECCV*, 2020.

- [21] Guocheng Qian, Jinjie Mai, Abdullah Hamdi, Jian Ren, Aliaksandr Siarohin, Bing Li, Hsin-Ying Lee, Ivan Skorokhodov, Peter Wonka, Sergey Tulyakov, and Bernard Ghanem. Magic123: One image to high-quality 3d object generation using both 2d and 3d diffusion priors. In *ICLR*, 2024.
- [22] Elad Richardson, Gal Metzer, Yuval Alaluf, Raja Giryes, and Daniel Cohen-Or. Texture: Text-guided texturing of 3d shapes. In *SIGGRAPH*, 2023.
- [23] Shunsuke Saito, , Zeng Huang, Ryota Natsume, Shigeo Morishima, Angjoo Kanazawa, and Hao Li. Pifu: Pixel-aligned implicit function for high-resolution clothed human digitization. In *ICCV*, 2019.
- [24] Shunsuke Saito, Tomas Simon, Jason Saragih, and Hanbyul Joo. Pifuhd: Multi-level pixel-aligned implicit function for high-resolution 3d human digitization. In *CVPR*, 2020.
- [25] Yichun Shi, Peng Wang, Jianglong Ye, Long Mai, Kejie Li, and Xiao Yang. Mvdream: Multi-view diffusion for 3d generation. *arXiv:2308.16512*, 2023.
- [26] Stanislaw Szymanowicz, Christian Rupprecht, and Andrea Vedaldi. Splatter image: Ultra-fast single-view 3d reconstruction. In *CVPR*, 2024.
- [27] Jiayang Tang, Zhaoxi Chen, Xiaokang Chen, Tengfei Wang, Gang Zeng, and Ziwei Liu. Lgm: Large multi-view gaussian model for high-resolution 3d content creation. *arXiv preprint arXiv:2402.05054*, 2024.
- [28] Peng Wang and Yichun Shi. Imagedream: Image-prompt multi-view diffusion for 3d generation, 2023.
- [29] Yuliang Xiu, Jinlong Yang, Xu Cao, Dimitrios Tzionas, and Michael J. Black. ECON: Explicit Clothed humans Optimized via Normal integration. In *CVPR*, 2023.
- [30] Yuliang Xiu, Jinlong Yang, Dimitrios Tzionas, and Michael J. Black. ICON: Implicit Clothed humans Obtained from Normals. In *CVPR*, 2022.
- [31] Dejie Xu, Ye Yuan, Morteza Mardani, Sifei Liu, Jiaming Song, Zhangyang Wang, and Arash Vahdat. Agg: Amortized generative 3d gaussians for single image to 3d. *arXiv preprint 2401.04099*, 2024.
- [32] Xiangyu Xu, Lijuan Liu, and Shuicheng Yan. Smpler: Taming transformers for monocular 3d human shape and pose estimation. *PAMI*, 2024.
- [33] Yinghao Xu, Hao Tan, Fujun Luan, Sai Bi, Peng Wang, Jiahao Li, Zifan Shi, Kalyan Sunkavalli, Gordon Wetzstein, Zexiang Xu, and Kai Zhang. Dmv3d: Denoising multi-view diffusion using 3d large reconstruction model, 2023.
- [34] Xueting Yang, Yihao Luo, Yuliang Xiu, Wei Wang, Hao Xu, and Zhaoxin Fan. D-if: Uncertainty-aware human digitization via implicit distribution field. In *ICCV*, 2023.
- [35] Xu Yinghao, Shi Zifan, Yifan Wang, Chen Hansheng, Yang Ceyuan, Peng Sida, Shen Yujun, and Wetzstein Gordon. Grm: Large gaussian reconstruction model for efficient 3d reconstruction and generation, 2024.
- [36] Tao Yu, Zerong Zheng, Kaiwen Guo, Pengpeng Liu, Qionghai Dai, and Yebin Liu. Function4d: Real-time human volumetric capture from very sparse consumer rgbd sensors. In *CVPR*, 2021.
- [37] Lvmin Zhang, Anyi Rao, and Maneesh Agrawala. Adding conditional control to text-to-image diffusion models. In *ICCV*, 2023.
- [38] Richard Zhang, Phillip Isola, Alexei A Efros, Eli Shechtman, and Oliver Wang. The unreasonable effectiveness of deep features as a perceptual metric. In *CVPR*, 2018.
- [39] Zechuan Zhang, Li Sun, Zongxin Yang, Ling Chen, and Yi Yang. Global-correlated 3d-decoupling transformer for clothed avatar reconstruction. In *NIPS*, 2023.
- [40] Zechuan Zhang, Zongxin Yang, and Yi Yang. Sifu: Side-view conditioned implicit function for real-world usable clothed human reconstruction. In *CVPR*, 2024.
- [41] Shunyuan Zheng, Boyao Zhou, Ruizhi Shao, Boning Liu, Shengping Zhang, Liqiang Nie, and Yebin Liu. Gps-gaussian: Generalizable pixel-wise 3d gaussian splatting for real-time human novel view synthesis. In *CVPR*, 2024.
- [42] Zerong Zheng, Tao Yu, Yebin Liu, and Qionghai Dai. Pamir: Parametric model-conditioned implicit representation for image-based human reconstruction. In *PAMI*, 2021.

A Appendix / Supplementary Materials

Experimental Environment. We conduct all the experiments on NVIDIA RTX A6000 GPU. The experimental environment is PyTorch 2.2.1 and CUDA 12.2.

Network structures. Our UNet model consists of 6 down blocks, 1 middle block, and 5 up blocks, with an input image size of 512×512 and an output Gaussian feature map size of 256×256 . We use 2 input views, resulting in a total of $256 \times 256 \times 4 = 131,072$ output Gaussians. Each block contains several residual layers and an optional down-sample or up-sample layer. For the last 3 down blocks, the middle block, and the first 3 up blocks, we insert cross-view self-attention layers after the residual layers. The final feature maps are processed by a 1×1 convolution layer to produce 14-channel pixel-wise Gaussian features. We adopt SiLU activation and group normalization for the UNet. Our Tr_{smpl} and Tr_{mix} share the same structure, consisting of multiple self-attention blocks. Specifically, they each have 5 up blocks and 5 down blocks. The down-sample channels are [64, 128, 256, 512, 1024], and the up-sample channels are [1024, 512, 256, 128, 64]. The input dimensions for Tr_{smpl} and Tr_{mix} are 35 and 256, respectively. The output dimension for both is 14, matching the dimension of the Gaussian features. For the attention blocks, we use a memory-efficient attention implementation.

Ablation visualization for SMPL guidance. We visualize the rendered images using only UNet without SMPL guidance and those produced by our full model, as shown in Fig. 7. Without SMPL guidance, the side view images exhibit significant artifacts, such as misaligned arms and unnatural shapes of clothes and heads, highlighted in the red boxes. This demonstrates the effectiveness of our SMPL-guided Gaussian prediction design.

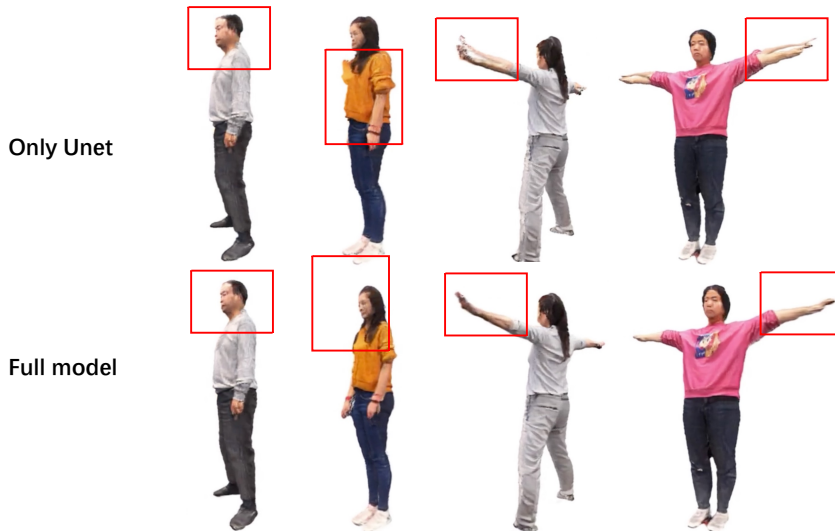


Figure 7: Ablation studies in terms of SMPL guidance. Details are highlighted in the red boxes.